Progress In Electromagnetics Research, PIER 84, 173–188, 2008

DESIGN OF BEAM-FORMING NETWORKS FOR SCANNABLE MULTI-BEAM ANTENNA ARRAYS USING CORPS

M. A. Panduro

Unidad Académica Multidisciplinaria Reynosa-Rodhe
Universidad Autónoma de Tamaulipas (UAT)
Carretera Reynosa-San Fernando
Reynosa, Tamaulipas, 88779, México

C. del Rio Bocio

Universidad Pública de Navarra
campus Arrosadia 31006, Pamplona, España

Abstract—This paper deals with the design of beam-forming networks (BFN) for scannable multibeam antenna arrays using Coherently Radiating Periodic Structures (CORPS). This design of CORPS-BFN considers the optimization of the complex inputs of the feeding network by using the Differential Evolution (DE) algorithm. Simulation results for different configurations of CORPS-BFN for a scannable multibeam linear array are presented. The results shown in this paper present certain interesting characteristics in the array factor response for the scannable multibeam linear array and the feeding network simplification for the design of BFN based on CORPS.

1. INTRODUCTION

Modern antenna applications such as MIMO Systems, Smart Antennas, Phased Antenna Arrays, etc., require the capability to handle several beams independently.

In this work, it is introduced the CORPS (Coherently Radiating Periodic Structures) concept to design BFN (Beamforming Networks) for multibeam antenna systems.

The philosophy of CORPS [1–4] has been presented in several papers. In these papers, it has been illustrated the CORPS network as a key methodology to feed antenna arrays [3]. In [3], it has been

considered the design of CORPS-BFN for antenna arrays of unique beam.

In this paper, it is introduced an innovative way to analyze a CORPS-BFN for scannable multibeam antenna arrays. In this case, due to the predefined features of the CORPS-BFN introduced, the amplitude and phase excitations should be introduced to the network and not to the radiating elements, as usual. These amplitude and phase excitations are determined by using the method of Differential Evolution (DE). Due to the nonlinear and nonconvex dependence of the parameters involved, the determination of the amplitude and phase excitations becomes a highly complex problem. However, DE has proven to be a fast and efficient algorithm for complex real-valued problems [5–9].

The main objective of this paper is to combine this new technology based on CORPS to define the BFN and the DE to look for optimal excitations, in order to generate a scannable multibeam linear array. The contribution of this paper is to present a perspective of the design of CORPS-BFN considering scannable multibeam linear arrays.

The remainder of the paper is organized as follows. Section 2 states the working principle that governs CORPS ideal behavior. Section 3 presents a description of the objective function used by the evolutionary algorithm; then experimental setup and the simulation results are presented in Section 4. Finally, the conclusions of this work along with some future line of research are presented in Section 5.

2. BEHAVIOR OF THE CORPS BEAMFORMING NETWORK

The working principle of the CORPS concept to feed antenna arrays has been explained in [3]. In this section we will try to illustrate the behavior of the CORPS-BFN for scannable multibeam linear arrays based on the previous work presented in [3].

A schematic representation of a CORPS-BFN of n inputs, N outputs and 3 layers is presented in Fig. 1. As shown in Fig. 1, a CORPS-BFN is conformed by a mesh interconnected by means of Split (S)-nodes and Recombination (R)-nodes.

The CORPS-BFN works as follows. The signal entered by one input port is divided in two and added with the arriving signals of the neighboring input ports. Following the path of each signal, we will find something like an inverted triangle (see Fig. 2) which has the lower vertex at the input port. The opposite side of this vertex will define the output ports receiving some information from this input port, or in other words, the effective radiating area from which every

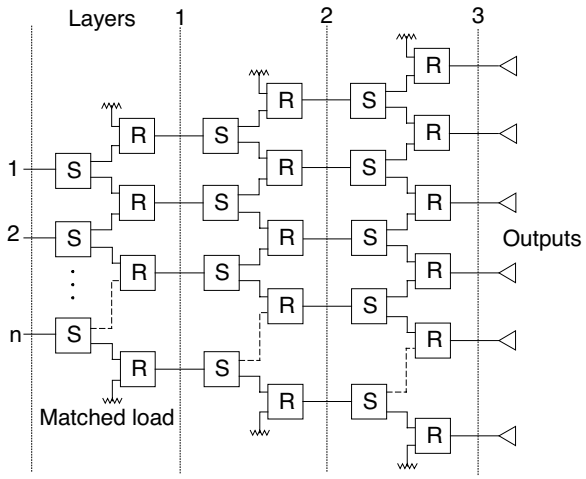

Figure 1. Schematic representation of a CORPS-BFN with S and R nodes.

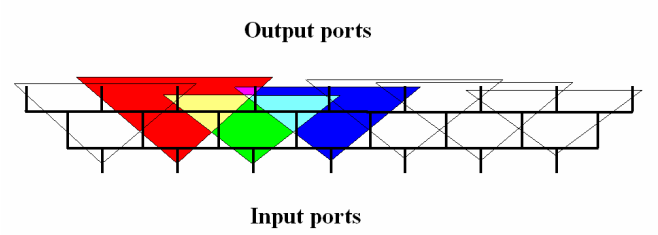

Figure 2. Path of each signal entered by one input port in the CORPS-BFN.

input signal (or orthogonal beam) will be radiated. Since the isolation between the input ports is ensured and the spreading of the signal inside the structure is controlled, the CORPS-BFN is able to handle simultaneously several orthogonal beams without any problem. In the outermost branches, the inputs that are not used are finished with a matched load in order to avoid reflections.

From [3] it could be extracted the Unitary Cell Scattering matrix that represent the behavior of a S-node, as follows.

$$[S] = \begin{bmatrix} 0 & j/\sqrt{2} & j/\sqrt{2} \\ j/\sqrt{2} & 0 & 0 \\ j/\sqrt{2} & 0 & 0 \end{bmatrix} \tag{1}$$

It is also shown in this paper that an S-node can act also like an R-

node. In the same way, we can use

$$V^- = SV^+ \tag{2}$$

in order to evaluate the fields after a S-node or R-node. In (2) S is the Scattering Matrix of an S-node and V^+ is the Amplitude and Phase of the field at input ports of an S-node. Using (2) and the schematic representation of a CORPS-BFN (Fig. 1) it is possible to establish an iterative code (i.e., with MATLAB) that represent the propagation of signal throughout a general configured CORPS-BFN.

As illustrated in the schematic representation, it is possible to establish many configurations for the CORPS-BFN with different number of inputs, outputs and layers. In this case, several orthogonal beams could be generated simultaneously by intercalating or interleaving the inputs of the CORPS-BFN, i.e., a group of different inputs will generate the beam # 1 and another group of inputs could generate another beam (i.e., the beam # 2). Following the philosophy of CORPS, each group of inputs must be established in a strategic way in order to have the capability to control electronically the corresponding beam pattern (over a scanning range) with a smaller number of complex inputs with respect to the number of antenna elements employed. Several configurations for the CORPS-BFN could be evaluated and studied. To set an example, the next configurations could be of interest.

1) For a system of 24 radiators and 23 input ports (i.e., a CORPS-BFN of one layer), a signal could be defined by the first 12 of the 23 input ports, and the resting 11 be used for another orthogonal signal, being both scanned towards different directions (see the Fig. 3). As illustrated in the Fig. 3, the group of 12 inputs could control to 13 of 24 radiators, and the resting 11 could control to 12 radiators.

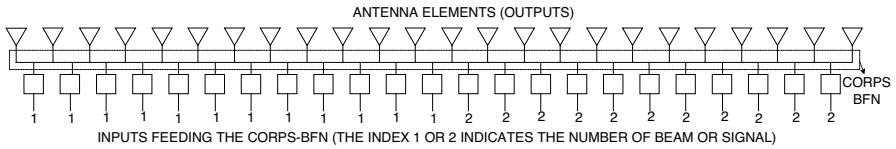

Figure 3. System of 24 radiators and 23 input ports with 12 complex inputs to control 13 radiators (beam # 1) and 11 complex inputs to control 12 antennas (beam # 2).

2) For the same system, two orthogonal beams could be generated simultaneously by intercalating the inputs of the CORPS-BFN, as

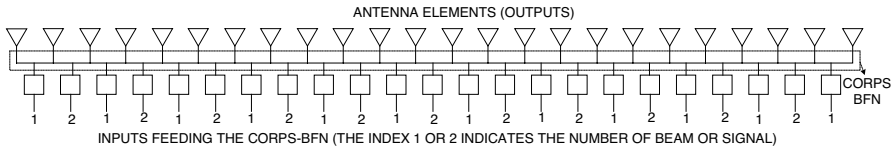

Figure 4. System of 24 radiators and 23 input ports with 12 complex inputs to control 24 antennas (beam # 1) and 11 complex inputs to control 22 antennas (beam # 2).

shown in the Fig. 4. The interesting of this case is that the group of 12 inputs (that generates the beam # 1) could control the 24 radiators of the array, and the resting 11 (used for the beam # 2) control to 22 of 24 radiators.

3) For the system of 24 radiators, we could use a CORPS-BFN of two layers with 22 input ports. Two orthogonal beams could be generated simultaneously by intercalating the inputs of the CORPS-BFN by pairs as illustrated in the Fig. 5. In the case of the beam # 1, 12 of 22 input ports could control 24 radiators of the array. For the beam # 2, the resting 10 control to 20 of 24 radiators.

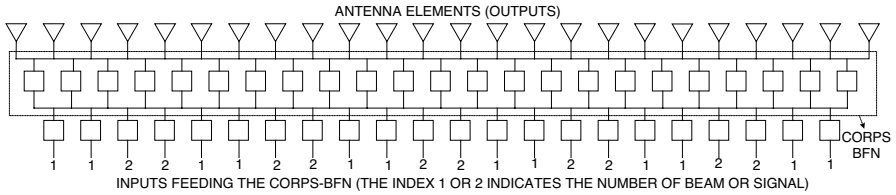

Figure 5. System of 24 radiators and 22 input ports with 12 complex inputs to control 24 antennas (beam # 1) and 10 complex inputs to control 20 antennas (beam # 2).

For a set of complex inputs [**a**] feeding the CORPS-BFN, the characteristics of Directivity (D) and Side Lobe Level (SLL) for each beam pattern can be calculated using the equation of the array factor as [10–14]

$$AF(\theta, \mathbf{a}) = \sum_{n=1}^{N} b_n \exp(jkd_n \cos\theta) \tag{3}$$

where b_i represents the complex excitation of the ith antenna element of the array, d_n represents the position of the antenna element n,

$k = 2\pi/\lambda$ is the phase constant and θ is the angle of incidence of a plane wave, λ is the signal wavelength.

In this case, the complex inputs feeding the CORPS network are given by

$$a_i = A_i \exp(j\phi_i) \cdot \exp(j\psi_i) \quad for \quad 1 \leq i \leq N - L \tag{4}$$

where L is the number of layers of the CORPS network and

$$\psi_i = kdm_i \cos\theta_0 \tag{5}$$

with

$$dm_i = d_i + \frac{(N-1)}{(N-1) - L} \tag{6}$$

Please, note that dm_i is not a design parameter. The idea of setting $\exp(j\psi_i)$ is to set a phase excitation in the complex inputs of the feeding network as a result of the linear interpolation of a conventional progressive phase excitation. The objective of setting this phase excitation is that the optimization algorithm searches possible phase perturbations that generate an optimal array factor with angles of the main beam near the desired direction.

The objective function and the evolutionary optimization technique used to optimize the complex inputs of the CORPS-BFN are described in the next section.

3. OBJECTIVE FUNCTION AND THE TECHNIQUE USED

One of the latest evolutionary computational techniques is the DE algorithm, in which, some individuals are randomly extracted from the solution population and geometrically manipulated [6], avoiding the destructive mutation of Genetic Algorithms (GA) [15–22]. The most prominent advantage of DE is its low computation time compared to that of GA. DE is an alternative to speed up the GA. Instead of small alterations of genes in GA mutation, DE mutation is performed by means of combinations of individuals [6].

First an initial population is formed in which the chromosomes have a Gaussian distribution. For each vector or solutions (amplitude and phase perturbations of the complex inputs feeding the CORPS-BFN) of the population $(N_p)X_i$, $i = 1, 2, \ldots, N_p$ of the G_{th} iteration, two new trial members, ε_{t1} and ε_{t2}, are generated as follows:

$$\varepsilon_{t1} = \varepsilon_{r1}^{(G)} + F\left(X_i^{(G)} - \varepsilon_{r2}^{(G)}\right) \tag{7}$$

$$\varepsilon_{t2} = \varepsilon_{r1}^{(G)} + F\left(X_i^{(G)} - \varepsilon_{r3}^{(G)}\right) \tag{8}$$

where $F \in [0, 2]$ is a real constant factor range suggested in [23], which controls the amplification of the differential variation, and the integers r_1, r_2, $r_3 \in [1, N_p]$ are randomly chosen such that $r_1 \neq r_2 \neq r_3$.

In this case each individual generates an array factor of certain characteristics of the side lobe level and the directivity. Therefore, the design problem is formulated as minimize the next objective function

$$\textit{Obj-fun} = (|AF(\theta_{SLL}, \mathbf{a})| / \max|AF(\theta, \mathbf{a})|) + (1/D(\theta, \mathbf{a})) \tag{9}$$

where θ_{SLL} is the angle where the maximum side lobe is attained. In this case both objectives (SLL and D) are uniformly weighted in the cost function.

After the objective function evaluation, the best solution in the set $\{\varepsilon_i, \varepsilon_{t1}, \varepsilon_{t2}\}$ becomes the new member for the next iteration, ε_i^{G+1}. Some chromosomes in the new population occasionally generate array factors which are not physically realizable, and an adjusting process is needed [7]. Taking the best solution into account, a termination criterion is proposed by fixing a number of iterations without an improvement over this solution. Storn and Prince [8] explain the procedures involved at each step of this algorithm in detail.

The next section presents the results for the configurations illustrated in the Section 2 using the DE algorithm.

4. SIMULATION RESULTS

The DE algorithm was implemented to study the behavior of the array factor generated by the configurations shown in the Section II of a CORPS-BFN for scannable multibeam linear arrays. The experiments parameters were set as follows: maximum number of generations $r_{\max} = 500$, population size $N_p = 200$, and $F = 0.5$ [23]. The obtained results are explained below.

Figure 6 illustrates the behavior of the array factor generated by the system of 24 radiators and 23 input ports with 12 complex inputs to control 13 antennas (beam # 1) and 11 complex inputs to control 12 antennas (beam # 2) (configuration 1 shown in the Fig. 3). In this case, the direction of maximum radiation is set in $\theta_0 = 70°$ for the beam # 1 and $\theta_0 = 110°$ for the beam # 2.

As shown in the Fig. 6, two simultaneous beams of different signals could be generated by such CORPS-BFN. This figure illustrates that the amplitude and phase excitations feeding the CORPS-BFN optimized by the DE algorithm can achieve a good performance in the two beams radiation.

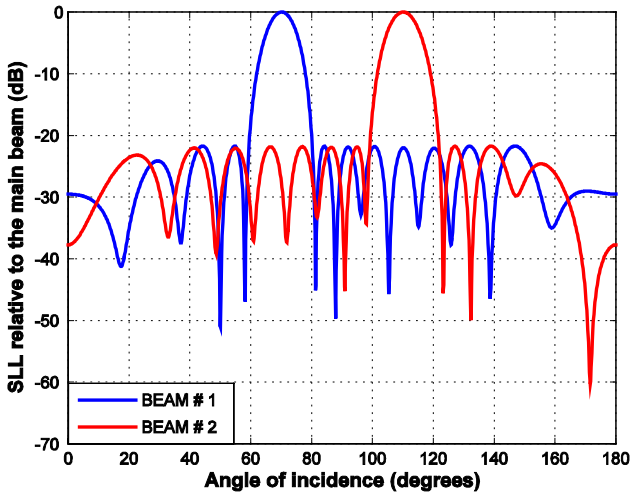

Figure 6. Array factor generated by the configuration 1 illustrated in the Fig. 3 (the direction of maximum radiation is set in $\theta_0 = 70°$ for the beam # 1 and $\theta_0 = 110°$ for the beam # 2).

Table 1 illustrates numerical values of the *SLL*, *D*, and the amplitude and phase perturbation distributions for the array factor generated. This table shows the evaluation of the array factor considering the scanning range of $50° \leq \theta_0 \leq 130°$, with an angular step of 10°. As shown in the Table 1, the amplitude and phase perturbation distributions optimized by the DE algorithm generates two scannable simultaneous beams with a maximum performance in terms of the *SLL* and *D* in all scanning range.

This particular configuration only permits to control a subset of antenna elements of the array for each beam pattern. However, desired characteristics of the *SLL* could be remained in a wide scanning range. Note, that the two scannable beams are generated with $N-1$ complex inputs feeding the CORPS-BFN.

Figure 7 shows the array factor for the case of the configuration 2 (Fig. 4), the system of 24 radiators and 23 input ports. In this case, a group of 12 complex inputs controls 24 antennas (beam # 1), and the resting 11 control to 22 antennas (beam # 2) of the array. This figure illustrates the case when the direction of maximum radiation is set in $\theta_0 = 80°$ for the beam # 1 and $\theta_0 = 100°$ for the beam # 2. As shown in the Fig. 7 the characteristics of the *SLL* for the two beams generated degrade with respect to the previous case. The numerical values of the *SLL*, *D* and the complex inputs distributions for the two

Table 1. Numerical values of *SLL*, *D* and the amplitude and phase perturbation distributions for the array factor generated by the configuration 1, (Fig. 3) in a scanning range of $50° \leq \theta_0 \leq 130°$.

BEAM # 1				
θ_0	***SLL*(dB)**	***D*(dB)**	**Amplitude distribution**	**Phase perturbation distribution (deg)**
50º	-17.43	9.78	8.5911, 11.0503, 6.7735, 9.9067, 7.8293, 6.6887, 12.2372, 10.2686, 8.4219, 7.2292, 12.8308, 11.9815	47.276, 27.836, 15.836, 16.914, 30.664, 50.6375, 63.3224, 74.6844, 88.575, 91.3056, 84.47, 62.207
60º	-19.24	10.28	12.4523, 11.8635, 12.9898, 7.0186, 6.9425, 9.3275, 7.4239, 10.2234, 11.8723, 7.8814, 9.8670, 9.3818	154.68, 118.41, 97.484, 143.698, 166.791, 151.79, 143.693, 160.516, -176.27, -169.345, -172.626, 160.5
70º	-21.72	10.56	8.3563, 12.3118, 6.4972, 10.6783, 6.2798, 8.9393, 9.6719, 9.1893, 9.5446, 9.8563, 8.2810, 10.0724	167.737, 128.442, 152.92, 172.36, 154.09, 172.345, -179.36, 174.11, -173.49, -171.14, -149.17, 178.858
80º	-19.78	10.80	7.5407, 6.1949, 6.1573, 9.5757, 9.7358, 6.2409, 7.69, 6.3632, 13.7386, 13.1631, 13.8059, 8.5971	4.58, -37.355, 15.9, -0.3467, -13.3116, 23.176, 11.534, -17.7, 33.027, -8.805, 56.4126, 4.4427
90º	-20.08	10.89	13.7247, 6.9244, 13.9496, 11.2913, 9.2014, 10.03, 12.2122, 9.1137, 9.8995, 10.9443, 12.2576, 9.4469	13.7094, 27.0517, 5.9598, 31.22, 0.4484, 23.424, 8.6155, 13.594, 7.9516, 16.6178, 2.2191, 12.1064
100º	-19.93	10.80	13.4957, 6.1176, 8.6593, 11.0579, 9.9784, 12.6786, 11.88, 8.043, 13.0799, 10.316, 13.1934, 12.9277	-177.98, 179.998, -167.86, 167.6, 176.9, -176.44, 164.59, -173.9, 144.74, -168.764, 109.8, 176.03
110º	-18.62	10.59	12.6833, 6.1131, 6.1508, 9.3537, 13.5372, 13.9099, 13.8627, 8.6308, 10.9388, 6.221, 12.9785, 8.4202	-164.29, -130.79, -177.58, -156.6, -131.79, 154.55, -170.85, -140.408, 153.32, 162.36, 172.75, -174.9
120º	-18.61	10.30	11.6137, 13.1837, 12.7359, 10.9207, 8.2865, 12.53, 9.1466, 6.4321, 13.1029, 6.0646, 6.1252, 11.3685	55.553, 86.62, 102.704, 66.545, 47.499, 50.8736, 54.652, 54.4736, 31.482, 2.474, 11.222, 47.854
130º	-17.58	9.78	6.068, 7.464, 13.7943, 13.7178, 12.1144, 12.0046, 11.6038, 8.6123, 6.1303, 6.0672, 6.2923, 6.4712	47.6844, 69.7648, 80.062, 73.8958, 62.2125, 47.6697, 35.4965, 17.025, 3.179, 7.2027, 17.0284, 33.7782
BEAM # 2				
θ_0	***SLL*(dB)**	***D*(dB)**	**Amplitude distribution**	**Phase perturbation distribution (deg)**
50º	-16.97	9.45	11.9386, 6.1391, 13.5811, 8.2353, 7.0658, 10.0391, 11.9345, 13.6086, 6.5949, 13.1684, 6.6707	19.889, -1.0673, -9.7634, -11.0472, -2.548, 22.9949, 48.9045, 62.158, 61.1508, 49.343, 30.7403
60º	-18.17	9.95	7.2456, 12.3708, 11.3939, 12.6039, 11.6813, 9.1964, 12.6888, 13.1999, 11.7067, 13.5629, 7.801	173.798, 136.78, 115.96, -169.94, -170.97, 166.584, 155.37, -153.57, -131.1373, -149.152, 177.95
70º	-19.01	10.29	12.0176, 13.2991, 6.9987, 10.9438, 9.7529, 8.5864, 6.9119, 11.9591, 10.32, 12.3808, 8.5201	-176.115, 158.252, 164.657, -178.825, 174.3, -163.214, -172.64, -170.33, -163.6, -129.92, -173.43
80º	-19.56	10.48	6.8334, 10.572, 13.2548, 12.3054, 9.9257, 10.9447, 7.3167, 11.7629, 13.1583, 10.5063, 12.6647	161.549, 102.84, 178.383, 134.29, -177.7, 149.831, 176.503, 174.331, 147.4244, -153.9463, 163.72
90º	-19.23	10.53	6.0473, 6.5117, 12.6359, 6.0009, 12.2965, 11.19, 12.3839, 6.9184, 11.1194, 13.5256, 8.3887	-5.9324, 35.3131, -8.594, 13.359, -9.7015, 4.7599, -10.1038, 7.7872, -10.4369, 30.063, -8.9507
100º	-18.44	10.47	6.3915, 6.0796, 8.6748, 9.3104, 9.0863, 7.7988, 13.9628, 13.6495, 10.685, 7.873, 7.4388	178.656, 173.668, -167.891, 158.745, 175.12, 179.665, 167.788, 153.39, -158.896, 115.489, 176.784
110º	-21.74	10.20	9.6156, 9.1024, 6.0935, 13.222, 13.9146, 10.496, 8.139, 6.0719, 12.9013, 6.133, 13.843	179.324, -144.025, -175.597, -177.02, -161.57, 161.34, 171.14, -174.6, 150.379, 143.287, 179.714
120º	-18.11	9.95	7.3964, 9.6426, 9.7482, 7.365, 10.3029, 13.4493, 11.3568, 6.0567, 7.9285, 9.147, 9.0168	15.6075, 50.442, 72.636, -2.419, -3.343, 17.999, 38.415, -31.935, -39.3443, -19.8947, 11.0868
130º	-16.91	9.46	10.0207, 13.5824, 11.7354, 7.5993, 8.8607, 12.5575, 8.9954, 10.959, 11.4947, 7.8035, 6.8952	119.753, 138.033, 149.262, 153.674, 142.756, 115.204, 91.182, 77.45, 79.556, 89.894, 108.16

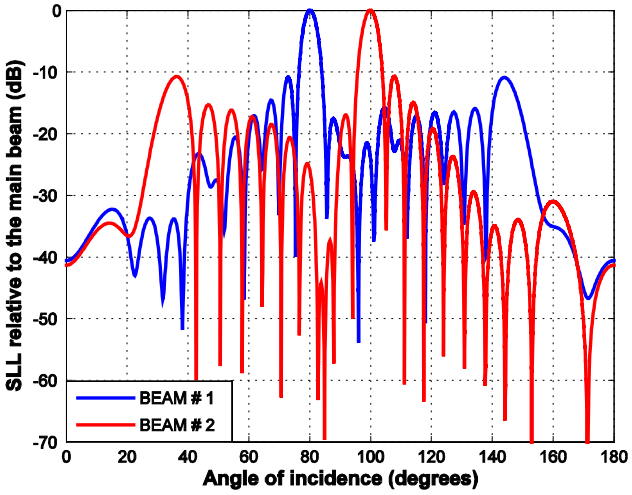

Figure 7. Array factor generated by the configuration 2 shown in the Fig. 4 (the direction of maximum radiation is set in θ_0 =80° for the beam # 1 and θ_0 =100° for the beam # 2).

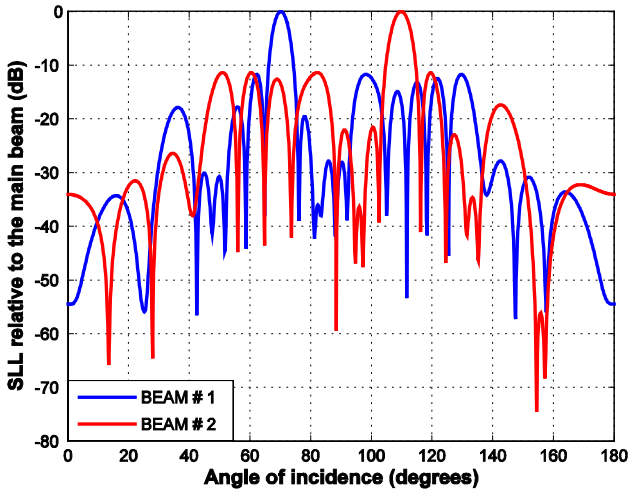

Figure 8. Array factor generated by the configuration 3 illustrated in the Fig. 5 (the direction of maximum radiation is set in $\theta_0 = 70°$ for the beam # 1 and $\theta_0 = 110°$ for the beam # 2).

scannable beams considering the scanning range of $70^\circ \leq \theta_0 \leq 110^\circ$ are illustrated in the Table 2. As illustrated in the Table 2, this configuration of CORPS-BFN presents a better performance in terms of *SLL* and *D* in angles near broadside and the possibilities of scanning are reduced.

For this configuration each beam pattern is controlled by $N/2$ complex inputs feeding the CORPS-BFN, i.e., it is feasible to control more antennas with respect to the last case making possible more directivity for the two scannable beams, as presented in the Table 2.

Table 2. Numerical values of *SLL*, *D* and the complex inputs distributions for the two scannable beams generated by the configuration 2, (Fig. 4) in a scanning range of $70^\circ \leq \theta_0 \leq 110^\circ$.

BEAM # 1				
θ_0	***SLL*(dB)**	***D*(dB)**	**Amplitude distribution**	**Phase perturbation distribution (deg)**
70^o	-3.87	11.37	9.0724, 7.9295, 8.74, 8.7147, 9.3068, 6.6449, 13.9363, 7.2018, 7.475, 13.5016, 8.039, 9.0471	145.654, 99.707, 110.009, 118.464, 128.35, 138.098, 147.804, 158.045, 167.39, 176.1, -173.654, 140.635
80^o	-10.87	12.71	6.0188, 13.9837, 6.0275, 9.6132, 7.9787, 13.9263, 7.7088, 6.3424, 13.6391, 13.9155, 13.8941, 8.9599	-100.031, -143.4, -123.5, -115.315, -104.99, -75.3, -81.96, -68.65, -71.55, -36.93, -35.96, -82.546
90^o	-23.91	13.33	8.0335, 6.4897, 11.8132, 7.3623, 12.4806, 6.9925, 13.3573, 7.2931, 8.2647, 7.6099, 6.2751, 13.1520	5.0589, 5.6375, 7.007, 5.5368, 6.2472, 6.7886, 5.883, 6.3343, 6.2454, 6.1409, 5.6473, 5.3645
100^o	-10.47	12.28	7.4873, 13.4721, 10.8983, 10.4066, 6.0287, 13.8694, 6.046, 8.7056, 13.8983, 6.1484, 12.9487, 6.0718	-57.565, 21.307, 12.67, 6.261, -9.589, -14.72, -20.374, -14.7446, -23.046, -43.2184, -57.1826, 15.91
110^o	-3.87	11.38	7.5794, 13.9937, 8.6734, 6.1369, 9.0704, 10.2158, 12.9623, 6.6739, 8.9286, 10.4758, 8.8853, 10.7673	17.2894, 63.0532, 53.09, 44.2042, 34.8222, 24.7253, 14.922, 5.418, -4.709, -13.324, -23.4694, 22.339
BEAM # 2				
θ_0	***SLL*(dB)**	***D*(dB)**	**Amplitude distribution**	**Phase perturbation distribution (deg)**
70^o	-4.61	11.27	8.8403, 13.056, 11.9554, 11.304, 10.6264, 12.4505, 8.9471, 10.6362, 9.6489, 6.8862, 6.5518	139.492, 98.46, 109.15, 118.5775, 128.93, 139.704, 150.344, 160.711, 170.1565, -179.104, 139.8915
80^o	-11.00	12.01	12.4969, 9.4072, 13.6817, 7.8163, 8.5389, 12.3112, 9.6382, 11.992, 11.5082, 7.1099, 13.1553	-124.64, 161.96, 175.28, -170.153, -162.93, -161.27, -158.29, -150.48, -137.28, -122.89, 162.041
90^o	-23.15	12.96	12.2636, 13.7867, 7.5969, 7.246, 9.8048, 11.3672, 8.9095, 11.3727, 7.6347, 7.1615, 6.3806	174.732, 175.479, 175.813, 175.78, 175.64, 175.737, 175.345, 176.083, 175.827, 175.119, 175.091
100^o	-10.73	12.50	7.2975, 12.1313, 11.9442, 10.4423, 6.7472, 11.6596, 12.0127, 6.0938, 13.7655, 13.46, 6.0509	-15.1435, 24.6173, 17.1832, 9.868, 3.3848, -1.9063, -7.5855, -13.9994, -21.322, -28.7504, 10.951
110^o	-4.61	11.27	13.4702, 12.7167, 9.5984, 12.742, 6.8637, 8.5997, 12.1358, 7.432, 13.0743, 7.6002, 6.935	21.1623, 62.048, 51.5095, 41.9436, 31.5239, 20.9407, 10.2641, -0.0637, -9.675, -20.3306, 20.661

Finally, Fig. 8 presents the behavior of the array factor generated by the system of 24 radiators and 22 input ports with 12 complex

Table 3. Numerical values of *SLL*, *D* and the complex inputs distributions for the two scannable beams generated by the configuration 3, (Fig. 5) in a scanning range of $60^\circ \leq \theta_0 \leq 120^\circ$.

BEAM # 1				
θ_0	***SLL*(dB)**	***D*(dB)**	**Amplitude distribution**	**Phase distribution (deg)**
60º	-4.52	10.57	8.9577, 13.893, 11.2665, 9.5325, 13.475, 11.0643, 13.2107, 10.851, 6.7175, 12.5381, 12.782, 7.0183	34.7815, -36.058, 14.498, -36.449, 53.584, 9.486, 98.213, 52.8585, 141.024, 91.47, 140.2016, 66.718
70º	-11.84	12.15	7.6904, 7.4786, 6.9623, 8.0085, 7.9375, 6.3158, 6.057, 10.9369, 13.8524, 10.4812, 8.4445, 13.917	120.09, 20.55, 73.786, 12.365, 109.865, 50.859, 139.331, 82.793, -167.969, 124.756, 178.21, 77.903
80º	-12.03	12.56	13.4652, 13.8795, 6.9769, 8.0301, 6.2766, 7.1847, 11.01, 9.9147, 12.6701, 9.2681, 6.227, 6.7267	72.362, 29.08, 138.104, 34.307, 81.686, 54.287, 86.309, 31.452, 100.7985, 43.437, 131.701, 71.082
90º	-10.17	12.18	13.9041, 7.3741, 6.2678, 10.9298, 12.8526, 6.1001, 13.8894, 12.6850, 10.2478, 8.4924, 9.0157, 13.8632	147.597, 141.25, -42.532, 146.09, 145.14, 146.051, 145.432, 151.857, 149.36, -48.1, 146.394, 151.42
100º	-12.00	12.77	12.1186, 13.3329, 11.8534, 8.584, 8.0038, 13.842, 11.5296, 10.1919, 9.0897, 10.1718, 11.6121, 6.6362	134.789, 172.869, 66.891, 157.716, 102.039, 154.74, 100.138, 154.817, 94.926, -174.7, 80.42, 119.88
110º	-11.82	12.17	9.5633, 9.9314, 8.8044, 8.2705, 10.1032, 8.6224, 13.6593, 13.7742, 6.9125, 11.7373, 6.0966, 6.1643	68.589, 165.776, 107.71, 169.5805, 66.8555, 127.558, 50.156, 96.782, -7.287, 55.361, 2.9858, 104.3936
120º	-4.53	10.55	12.0369, 8.5386, 10.7264, 13.902, 11.0941, 13.9629, 6.0651, 13.7079, 13.9257, 6.9966, 8.9958, 6.8816	70.334, 143.245, 93.014, 141.089, 52.083, 95.5, 3.826, 51.78, -34.684, 13.5648, -34.1795, 39.5229
BEAM # 2				
θ_0	***SLL*(dB)**	***D*(dB)**	**Amplitude distribution**	**Phase distribution (deg)**
60º	-4.22	9.86	6.3746, 6.8203, 9.0117, 6.547, 7.8815, 12.5566, 6.888, 13.5244, 10.5379, 7.1726	-68.215, -130.968, -72.955, -118.8998, -22.7485, -65.5882, 29.808, -16.574, 42.664, -22.0464
70º	-11.48	11.64	7.8289, 7.0798, 12.0208, 8.381, 13.9534, 9.5819, 13.6898, 13.2106, 7.7136, 12.9943	156.855, 73.349, 137.564, 80.6651, -176.4968, 129.166, -122.9977, 175.2746, -124.0137, 155.4348
80º	-11.86	12.07	12.4958, 12.2375, 6.8941, 13.1122, 12.8326, 7.9788, 12.6365, 10.2318, 8.668, 11.833	137.971, 96.845, -170.664, 111.369, 166.032, 117.438, 171.056, 95.744, -174.407, 144.453
90º	-10.05	11.66	13.1643, 13.1721, 11.8821, 10.9711, 10.9134, 6.9376, 11.1231, 6.6632, 12.1265, 9.3503	-178.328, -178.652, 161.362, -179.919, 179.835, 178.665, 178.27, 124.519, 177.976, 176.945
100º	-11.86	12.07	6.1545, 13.2, 6.3225, 11.4928, 12.6952, 8.0859, 13.4287, 8.0488, 11.7665, 11.7067	-144.22, -103.65, 166.27, -118.014, -171.925, -123.852, -177.678, -100.017, 167.338, -150.872
110º	-11.35	11.60	6.4238, 7.7004, 13.7997, 9.2843, 6.9957, 6.5042, 8.1577, 7.442, 13.1932, 8.5531	136.608, -139.333, 164.3095, -136.7297, 118.525, 175.355, 67.409, 127.2336, 67.205, 147.927
120º	-4.23	9.85	13.1956, 6.3114, 11.2961, 13.8949, 12.4604, 12.3343, 6.4269, 12.4206, 10.2709, 6.4096	-112.744, -48.592, -107.6015, -61.767, -155.771, -113.235, 149.955, -163.8605, 137.529, -158

inputs to control 24 antennas (beam # 1) and 10 complex inputs to control 20 antennas (beam # 2), i.e., the configuration 3 of the Fig. 5. For this case, the direction of maximum radiation is set in $\theta_0 = 70°$ for the beam # 1 and $\theta_0 = 110°$ for the beam # 2. From the Fig. 8, it could be observed that the possibilities of scanning are better for this configuration of CORPS-BFN with respect to the previous case. The interesting point is that these two scannable beams are generated with $N - 2$ complex inputs, i.e., one less complex input with respect to the configuration 2.

Table 3 shows the numerical values of the *SLL*, *D* and the complex inputs distributions for the two scannable beams considering the scanning range of $60° \leq \theta_0 \leq 120°$. From the Table 3, it is corroborated that the possibilities of scanning are better for this configuration of CORPS-BFN with respect to the previous case. However, it must be noted that the optimization of the complex inputs by using the DE algorithm achieves better characteristics of *SLL* and *D* for $\theta_0 = \{70°, 80°, 100°, 110°\}$ with respect to broadside.

Therefore, it is important to note that if the number of layers in the CORPS-BFN is increased and it is established the number of layers to be the same number of intercalating inputs for each beam pattern, the scanning performance improves, at the expense of increasing the side lobes and losing a little of the directivity at broadside.

As in the previous case, this configuration of CORPS-BFN permits to control more radiators with respect to the configuration 1, so, more directivity is achieved for the two scannable beams.

In this paper the idea was to demonstrate the possibilities of feeding an antenna array with a CORPS-BFN to generate scannable multiple beams. Although it was presented the case to generate two scannable beams, it is perfectly possible to define independently the number of input ports (defined by the number of orthogonal beams to be used simultaneously) and the number of radiating elements.

5. CONCLUSIONS

The design of beam-forming networks for scannable multibeam antenna arrays using CORPS has been presented. Simulation results reveal that the design of CORPS-BFN optimizing the complex inputs with the DE algorithm could generate scannable multiple beams with a significant simplification of the feeding network. The behavior of the array factor for different configurations of CORPS-BFN for a scannable multibeam linear array was studied and analyzed. Depending on the requirements of scanning, directivity and the simplification of the network the more convenient configuration could be established.

Despite, if the number of layers in the CORPS-BFN is increased and it is established the number of layers to be the same number of intercalating inputs for each beam pattern, the scanning performance improves, at the expense of increasing the side lobes and losing a little of the directivity at broadside.

Future work will deal with the design of CORPS-BFN for scannable multibeam planar (bi-dimensional) arrays and the study of new structures for designing BFN for multiple beam antenna systems.

ACKNOWLEDGMENT

This work was supported by the Mexican National Science and Technology Council, CONACyT, under grant J50839-Y and the Science and Technology Council of Tamaulipas Mexico (COTACyT) under Grant 2007-C13-73901.

REFERENCES

1. Panduro, M. A., "Design of coherently radiating structures in a linear array geometry using genetic algorithms," *AEU International Journal of Electronics and Communications*, Vol. 61, No. 8, 515–520, 2007.
2. Betancourt, D., A. Ibañez, and C. del Rio, "Designing antenna systems with CORPS," *28th ESA Antenna Workshop on Space Antenna Systems and Technologies, ESTEC*, Noordwijk, Holland, June 2005.
3. Betancourt, D. and C. del Río, "A novel methodology to feed phased array antennas," *IEEE Transactions on Antennas and Propagation*, Vol. 55, Issue 9, 2489–2494, September 2007.
4. Betancourt, D., A. Ibañez, and C. del Río, "Coherently radiating periodic structures (CORPS): A step towards high-resolution radiations systems," *IEEE AP-S 2005*, Washington, DC, 2005.
5. Kurup, D., M. Himdi, and A. Rydberg, "Synthesis of uniform amplitude unequally spaced antenna arrays using the differential algorithm," *IEEE Transactions on Antennas and Propagation*, Vol. 51, 2210–2217, 2003.
6. Feortisov, V. and S. Janaqui, "Generalization of the strategies in differential evolution," *Proceedings of the IEEE Conference Evolutionary Computation*, 1996.
7. Yang, S., A. Qing, and Y. B. Gan, "Synthesis of low side lobe antenna arrays using the differential evolution algorithm," *IEEE*

Transactions on Antennas and Propagation Conference, 1–22, 2003.

8. Storn, R. and K. Price, "Minimizing the real functions of the ICEC'96 contest by differential evolution," *Proceedings of the IEEE Conference Evolutionary Computation*, 1996.
9. Rocha-Alicano, C., D. Covarrubias-Rosales, C. Brizuela-Rodriguez, and M. A. Panduro_Mendoza, "Differential evolution applied to sidelobe level reduction on a planar array," *AEU International Journal of Electronics and Communications*, Vol. 61, 286–290, 2007.
10. Balanis, C., *Antenna Theory-Analysis and Design*, 2nd edition, Wiley, New York, 1997.
11. Kazemi, S. and H. R. Hassan, "Performance improvement in amplitude synthesis of unequally spaced array using least mean square method," *Progress In Electromagnetics Research B*, Vol. 1, 135–145, 2008.
12. Yuan, H. W., S. X. Gong, P. F. Zhang, and X. Wang, "Wide scanning phased away antenna using printed dipole antennas with parasitic element," *Progress In Electromagnetics Research Letters*, Vol. 2, 187–193, 2008.
13. Vescovo, R., "Beam scanning with null and excitation constraints for linear arrays of antennas," *J. of Electromagn. Waves and Appl.*, Vol. 21, No. 2, 267–277, 2007.
14. Lee, K. C. and J. Y. Jhang, "Application of particle swarm algorithm to the optimization of unequally spaced antenna arrays," *J. of Electromagn. Waves and Appl.*, Vol. 20, No. 14, 2001–2012, 2006.
15. Rahmat-Samii, Y. and E. Michielssen, *Electromagnetic Optimization by Genetic Algorithms*, Wiley & Sons, New York, 1999.
16. Panduro, M. A., D. H. Covarrubias, C. A. Brizuela, and F. R. Marante, "A multi-objective approach in the linear antenna array design," *AEU International Journal of Electronics and Communications*, Vol. 59, No. 4, 205–212, 2005.
17. Su, D. Y., D. M. Fu, and D. Yu, "Genetic algorithms and method of moments for the design of PIFAS," *Progress In Electromagnetics Research Letters*, Vol. 1, 9–18, 2008.
18. Nyobe, E. N. and E. Pemha, "Shape optimization using genetic algorithms and laser beam propagation for the determination of the diffusion coefficient in a hot turbulent jet of air," *Progress In Electromagnetics Research B*, Vol. 4, 211–221, 2008.
19. Sotiriou, A. I., P. T. Trakadas, and C. N. Capsalis, "Uplink

carrier-to-interference improvement in a cellular telecommunication system when a six-beam switched parasitic array is implemented," *Progress In Electromagnetics Research B*, Vol. 5, 303–321, 2008.

20. Mitilineos, S. A., "Genetic design of dual band, switched-beam dipole arrays, with elements failure correction, retaining constant excitation coefficients," *J. of Electromagn. Waves and Appl.*, Vol. 20, No. 14, 1925–1942, 2006.
21. Lei, J., G. Fu, L. Yang, and D. M. Fu, "Multiobjective optimization design of the Yagi-Uda antenna with an X-shape driven dipole," *J. of Electromagn. Waves and Appl.*, Vol. 21, No. 7, 963–972, 2007.
22. Zhai, Y. W., X. W. Shi, and Y. J. Zhao, "Optimized design of ideal and actual transformer based on improved micro-genetic algorithm," *J. of Electromagn. Waves and Appl.*, Vol. 21, No. 13, 1761–1771, 2007.
23. Parsopoulos, K. E., D. K. Tasoulis, N. G. Pavlidis, V. P. Plagianakos, and M. N. Vrahatis, "Vector evaluated differential evolution for multi-objective optimization," *IEEE Congress on Evolutionary Computation*, 19–23, 2004.